JOURNAL OF MATERIALS SCIENCE **39** (2004) 151–157

Temperature dependent complex permittivities of graphitized carbon blacks at microwave frequencies between 0.2 and 26 GHz

J. E. ATWATER*, R. R. WHEELER, JR.
UMPQUA Research Company, P.O. Box 609, Myrtle Creek, Oregon 97457, USA
E-mail: jatwater@urcmail.net

Many carbonaceous materials are amenable to dielectric heating at microwave frequencies. The primary indicator of microwave susceptibility is the complex permittivity (ε^*), of which, the real component correlates with polarization, and the imaginary term represents dielectric loss. For a given material, the complex permittivity is dependent upon both frequency and temperature. Here we report the complex permittivities over the frequency range from 0.2 to 26 GHz of four laboratory grade graphitized carbon blacks which are used as adsorbents and chromatographic media in a variety of separation, purification, and analytical applications. Measurements were made using a vector network analyzer based system across the temperature region between 23°C and 191°C. Dielectric polarization-relaxation phenomena are also characterized.

1. Introduction

Several forms of carbon black are highly susceptible to microwave (dielectric) heating. Among these are materials which are commonly used by analytical chemists and environmental scientists as adsorbents for the separation, concentration, and quantitation of various organic compounds. Graphitized carbon blacks are widely employed for the removal of contaminants from air [1] and water [2], as chromatographic media for quantitative analysis by gas chromatography [3–8], as solid phase extraction media for separation and concentration of organics from water samples prior to chromatographic analyses [9–15], and within guard columns used for high pressure liquid chromatography and ion chromatography [16, 17]. Susceptibility of these materials to dielectric heating may be used to advantage in the thermal regeneration of contaminant laden sorbents [18], in the direct heating of media within chromatography columns, and as a means for rapid volatilization of contaminants in purge and trap gas chromatography. However, much variability is evident between different forms of carbon black. To provide a quantitative view of the extent of this variability, complex permittivities of four laboratory grade graphitized carbon blacks were determined at microwave frequencies between 0.2–26 GHz, and over the temperature range between 23–191°C.

Dielectric heating through absorption of radiation at microwave frequencies involves phenomena such as induced electronic, atomic, and space charge polarizations, or the direct coupling of electromagnetic radiation with rotational and vibrational transitions of susceptible dielectric materials to produce heat. In non-magnetic media, susceptibility to microwave heating is governed by the frequency (ω) dependent complex permittivity [19, 20],

$$\varepsilon^*(\omega) = \varepsilon'(\omega) - i\varepsilon''(\omega) \tag{1}$$

The terms of ε^* are described by the Kramers-Kronig relations

$$\varepsilon'(\omega) = \varepsilon_\infty + \frac{2}{\pi}\int_o^\infty \frac{\varepsilon''(\omega)\omega'}{(\omega')^2 - \omega^2}\mathrm{d}\omega' \tag{2}$$

$$\varepsilon''(\omega) = \frac{2}{\pi}\int_o^\infty \frac{[\varepsilon'(\omega) - \varepsilon_\infty]\omega}{(\omega')^2 - \omega^2}\mathrm{d}\omega' \tag{3}$$

where ε_∞ is permittivity at the high frequency limit, and ω' is an integration variable [21]. In the complex plane, the real and imaginary terms of $\varepsilon^*(\omega)$ correlate with polarization, and energy loss, respectively. The loss factor or dissipation factor ($\tan\delta$) is defined as,

$$\tan\delta \equiv \frac{P_L}{P_S} = \frac{\omega\,\varepsilon''(\omega)|\mathbf{E}_o|^2}{\omega\,\varepsilon'(\omega)|\mathbf{E}_o|^2} = \frac{\varepsilon''(\omega)}{\varepsilon'(\omega)} \tag{4}$$

where the average power per unit volume (P_L) consumed by loss mechanisms is,

$$P_L = \frac{1}{2}\omega\varepsilon''|\mathbf{E}_o|^2 \tag{5}$$

*Author to whom all correspondence should be addressed.

and the average power stored due to dielectric polarization is,

$$P_S = \frac{1}{2}\omega\varepsilon'|\mathbf{E}_o|^2 \tag{6}$$

The attenuation of a microwave beam directed along the x-axis by an absorbing material is described by [22],

$$P(x) = P_o \exp(-2\alpha x) \tag{7}$$

where the attenuation coefficient (α) is a function of the angular frequency (ω), complex permittivity, and complex permeability (μ^*),

$$\alpha = \omega\sqrt{\sqrt{\varepsilon'^2 + \varepsilon''^2}\sqrt{\mu'^2 + \mu''^2}} \times \sin\left[\frac{\arctan\left(\frac{\varepsilon''}{\varepsilon'}\right) + \arctan\left(\frac{\mu''}{\mu'}\right)}{2}\right] \tag{8}$$

In non-magnetic materials, values of μ^* are extremely low, hence, microwave absorption is dominated by the complex permittivity terms. From this, it is clear that knowledge of the frequency and temperature dependencies of complex permittivity in the microwave region of the electromagnetic spectrum for specific materials may facilitate both the modeling and design of dielectric heating systems.

2. Experimental

The apparatus used to acquire complex permittivity data is illustrated schematically in Fig. 1. The integrated system consists of an HP8722D Vector Network Analyzer (VNA), an HP85070B Dielectric Probe, an HP85056A calibration kit, and an HP85130F adapter kit. While the HP8722D VNA was capable of operation between 0.05–40 GHz, limitations of the dielectric probe and associated transmission elements reduced the practical working frequency range to 0.2–26 GHz. Also, dissipation (tan δ) factors $\geq$0.05 are required to assure accuracy of the test results. Complex permittivity measurements were made under software control via a Hewlett-Packard Interface Bus (HPIB) parallel connection between the computer and the VNA. In operation, the VNA scans a preset frequency range over which transmission and reflection parameters are determined. Material in direct contact with the dielectric probe alters the phases and magnitudes of reflected power observed by the VNA. Complex permittivities were calculated from the measured transmission and reflection parameters using HP85071B software.

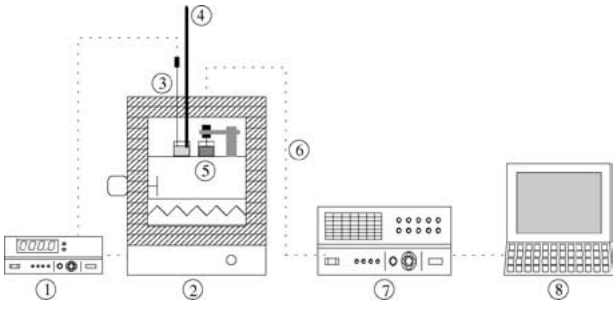

Figure 1 Complex permittivity test apparatus: (1) temperature controller, (2) oven, (3) thermocouple, (4) Hg thermometer, (5) dielectric probe immersed in sample, (6) high temperature semi-rigid coaxial cable, (7) vector network analyzer, and (8) computer.

To confirm the validity of complex permittivity data generated by this system, a series of aqueous 1,5-pentanediol solutions was examined at 25°C. Four solutions were analyzed, covering the full range of pentanediol mole fractions (χ) between 0–1. The data acquired in our laboratory were then compared to the recently published results of Wang *et al.* [23] which had been derived using substantially different methods based upon a circular waveguide/interferometric technique. Polarization relaxation times and static dielectric constants calculated from the VNA based complex permittivity data were in close agreement to the previously reported results.

To measure complex permittivities at elevated temperatures, the dielectric probe was mounted inside a gravity convection oven. To minimize temperature gradients, the oven was modified by sealing the external air convection current ports, and the addition of an internal recirculation fan. Improved temperature control was achieved using a digital PID controller and a K-type thermocouple probe mounted inside the oven. A 610 mm precision mercury thermometer covering the temperature range between −1°C to 201°C with 0.2°C resolution was used to monitor the temperature of the test specimen. Both the thermocouple probe and the mercury thermometer were inserted into a sand-filled beaker of equivalent volume and elevation within the oven as the material under study. A high temperature semi-rigid coaxial cable was used to connect the oven mounted dielectric probe with the external VNA. Access for the thermocouple, thermometer, and coaxial cable was established through a 5.0 cm diameter insulation filled circular opening at the top of the oven. Temperature regulation was accurate to within ±0.2°C.

The complex permittivities of four laboratory grade graphitized carbon blacks were determined. Details describing these materials are summarized in Table I. Measurements were performed at five temperatures covering the approximate range between 20–200°C. Samples were presented to the instrument as fine powders, thus obviating the need to correct for the effects of intergranular porosity [24–28]. To minimize interference from adsorbed water, each sample was dried at 180°C for a minimum of 72 h, and then stored in a dessicator prior to analysis. The instrument was first

TABLE I Summary of graphitized carbon black samples

Graphitized carbon black	Catalog no.[a]	Lot. no.	Mesh (US)	Surface area (m^2/g)
Carbopack B	2-0273	B-417	60–80	100
Carbopack C	2-0257	C-406	60–80	10
Carbopack X	1-0437	X-327	60–80	240
Carbopack Y	1-0462	Y-318	60–80	24

[a]Supelco, Bellefonte, Pennsylvania.

calibrated, followed by duplicate measurements at ambient temperature, with the dielectric probe in intimate contact with the material under study. The temperature was then increased. Once the set-point temperature was reached, a period of 45 min was allowed for the system to stabilize. Then a second set of duplicate measurements were made. This procedure was followed until data covering the full temperature span were gathered. The numerical values of all complex permittivities were calculated as dimensionless relative permittivities ($\varepsilon^*/\varepsilon_o$). These may be converted to absolute permittivities through multiplication by the permittivity of free space (ε_o), in appropriate units.

3. Results and discussion

Complex permittivities were determined at five temperatures between 23–191°C for Carbopack B, Carbopack C, Carbopack X, and Carbopack Y. The real and imaginary components of the complex permittivities for these four materials as functions of both frequency and temperature are presented in Figs 2–5, respectively.

3.1. Carbopack B

As indicated in Fig. 2, the relationship between the real term of the complex permittivity and frequency is represented by curves with strong sigmoidal character on the semi-logarithmic scale over the full temperature span. Values of ε' descend from maxima at the low frequency limit to minimum values at the 26 GHz high frequency cutoff for these experiments. Significant temperature dependence is observed over frequencies between 0.2–3 GHz. Above 3 GHz, the relationship between ε' and frequency is similar at all temperatures, although slight sinusoidal oscillation is evident above 10 GHz for the data gathered at 150.2°C and 190.7°C. These oscillations are most likely an artifact of the measurement process. Maximum values range between 175 and 215, and generally increase with temperature, with the exception that the ε' value for the experiment conducted at 23.8°C is slightly above that for 50.4°C. Minimum values of ε' converge at levels between 7–8 at 26 GHz.

The relationship between dielectric loss factor (ε'') and frequency is represented by a slightly distorted gaussian-like symmetry on the semilog scale. The frequencies of maximum loss range between 2.00–2.32 GHz, and generally decrease with increasing temperature. Values of ε'' range between 32.0 and 48.3 at 0.2 GHz, then rise to maxima which range between 83.7–101.2. ε'' generally increases with temperature over the frequency range between 0.2–2.2 GHz. At higher frequencies, cross-over between the data gathered at 23.8°C and 50.4°C occurs. For all temperatures, minimum values of ε'' converge to ≈18 at 26 GHz. Values for the dissipation factor (tan δ) are very weakly temperature dependent and rise monotonically from a minimum of ≈0.3 at 0.2 GHz and then plateau at a value of ≈2.5 over frequencies between 8–26 GHz.

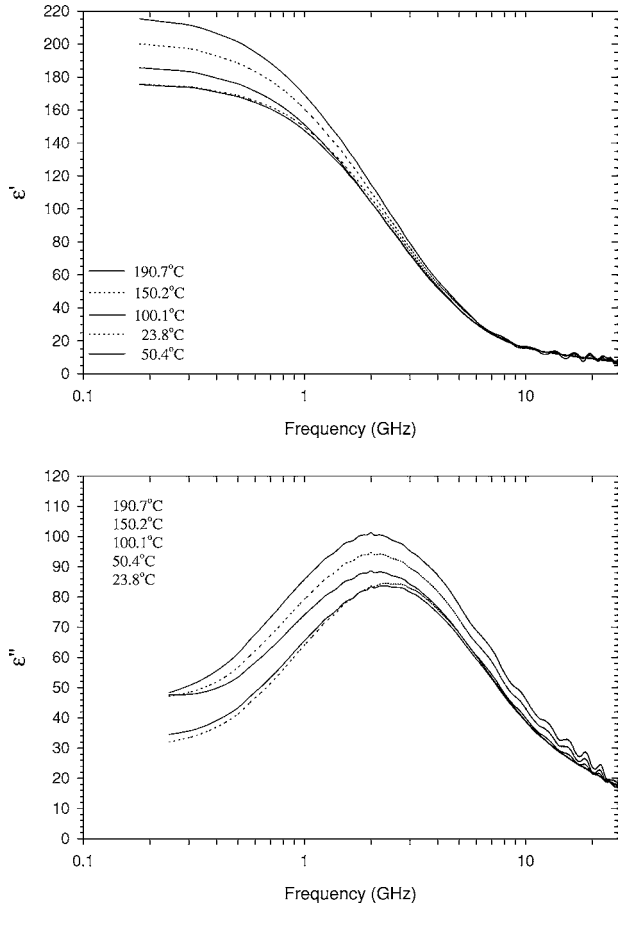

Figure 2 Carbopack B: real (ε') and imaginary (ε'') components of complex permittivity.

3.2. Carbopack C

For Carbopack C (Fig. 3), the same general symmetry is evident in the relationships between ε', ε'', and frequency as for the previous example (Fig. 2). However, the frequency of maximum dielectric loss is markedly shifted toward higher frequencies, and the sinusoidal oscillations at higher frequencies for data collected at the two highest temperatures are also more significant. At 0.2 GHz, ε' values vary between 155 and 194, then decrease sigmoidally to minimum values of ≈10 at 26 GHz. In general, ε' increases with temperature. Temperature dependence for ε' is strongest at low frequencies, and diminishes continuously with increasing frequency. Dielectric loss factors rise from between 9.0–16.2 at 0.2 GHz to maxima between 77.3 and 106.1 at the frequencies between 6.01 and 6.80 GHz. The strongest temperature effects on ε'' occur in the region surrounding the frequencies of maximum dielectric loss. In this region, both ε'' and the frequency of maximum loss increase significantly with temperature. Between 0.2–7 GHz, values of tan δ rise monotonically, with minimal temperature effects evident. At higher frequencies, the relative trends are obscured by the sinusoidal oscillations, although maximum dissipation factors of ≈3.6 are indicated.

3.3. Carbopack X

As indicated in Fig. 4, sigmoidal symmetry is less evident in the relationship between ε' and frequency

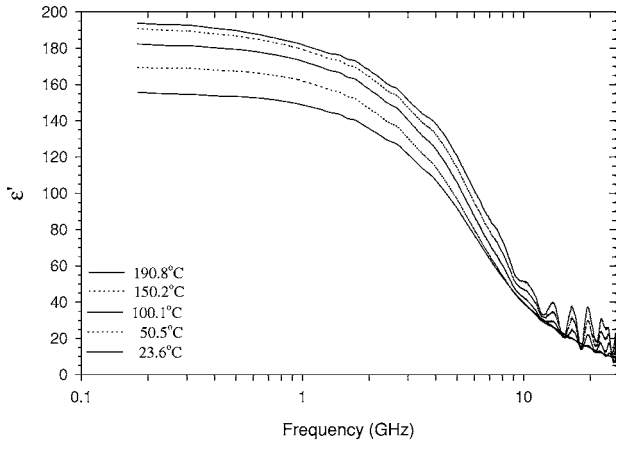

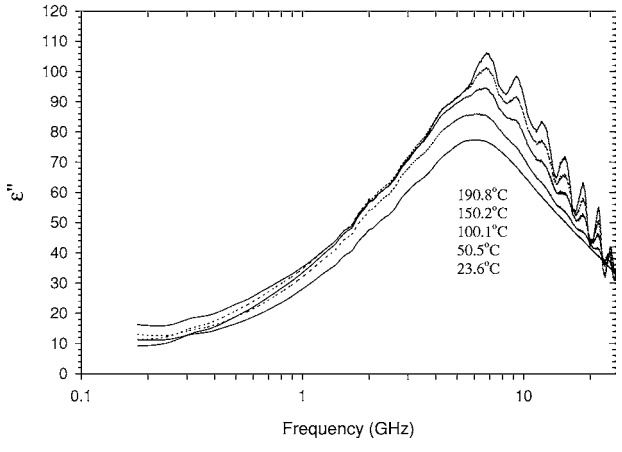

Figure 3 Carbopack C: real (ε') and imaginary (ε'') components of complex permittivity.

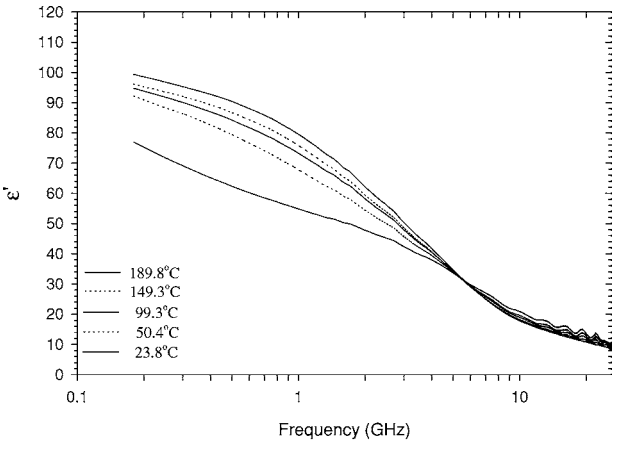

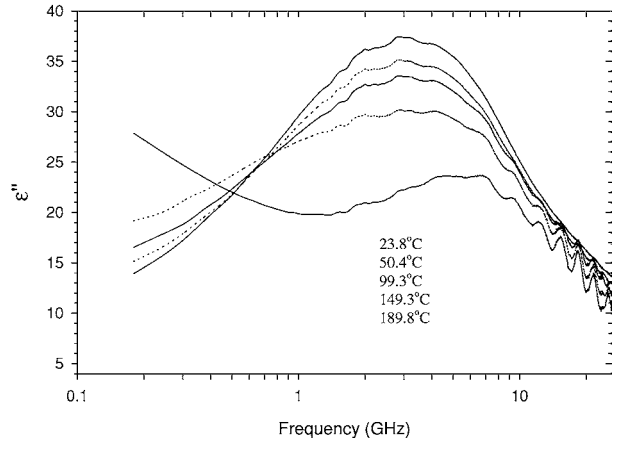

Figure 4 Carbopack X: real (ε') and imaginary (ε'') components of complex permittivity.

for this material. Maximum ε' values ranging between 77.0–99.4 occur at the 0.2 GHz low frequency limit and increase with temperature. ε' values diminish continuously with increasing frequency, exhibiting minimal temperature dependence above 4 GHz, and converge to minimum values of ≈8–10 at 26 GHz. Slight sinusoidal oscillations are present at frequencies above 10 GHz for temperatures between 99.3°C and 189.8°C. For temperatures between 23.8°C and 149.3°C, maximum dielectric loss factors occur at 2.90 GHz which vary between 30.2 and 37.4. In this region, the temperature trends evident in the previous two examples are reversed. Here, maximum dielectric loss varies inversely with temperature. At Frequencies below 0.7 GHz this trend is reversed. For example, at 0.2 GHz ε'' values increase steadily from 13.9 at 23.8°C to 27.9 at 189.8°C. With respect to dielectric loss, the data from the highest temperature point are somewhat anomalous. The frequency of maximum loss is shifted to 4.72 GHz, a value substantially higher than for the other temperatures. Also, a saddle point occurs between 1–2 GHz. At lower frequencies ε'' rises again toward a secondary maximum at 0.2 GHz. Dissipation factors rise steadily with frequency from minimum values ranging between 2–4 at 0.2 GHz to maxima between 1–1.6 at 26 GHz. For fixed frequencies above 1 GHz, dissipation factors vary inversely with temperature. This trend is reversed at the very lowest frequencies studied.

3.4. Carbopack Y

Anomalous results were obtained for Carbopack Y at the highest temperature point (188.9°C). For this reason, Fig. 5 presents ε', ε'', vs. frequency over the temperature span from 24.0°C to 150.1°C. Maximum ε' values occur at the low frequency limit and rise with temperature from 152 at 24°C to 165 at 150.1°C. At 0.3 GHz the high temperature curve crosses that of the lowest temperature. Above this frequency the temperature dependence of ε' does not follow clear trends. ε' data for all temperatures converge at frequencies above 7 GHz and reach minimum values of ≈5 at 26 GHz. Maximum dielectric loss ranging between 68.5–71.7 is evident at 2.00 GHz across the full temperature range. At 0.2 GHz ε'' values rise with temperature from 21.0 at 24.0°C to 47.2 at 150.1°C. Between 1–7 GHz the temperature trends become less clear. At frequencies above 7 GHz data from all temperatures converge toward minimum values of ≈14 which occur at 26 GHz. Values of tan δ rise monotonically with frequency to maximum values of approximately 2.6 which occur near 8 GHz. Temperature effects on tan δ are relatively minor across the full spectrum.

3.5. Polarization-relaxation phenomena

In susceptible solids, heat is produced via oscillating induced interfacial (Maxwell-Wagner) and

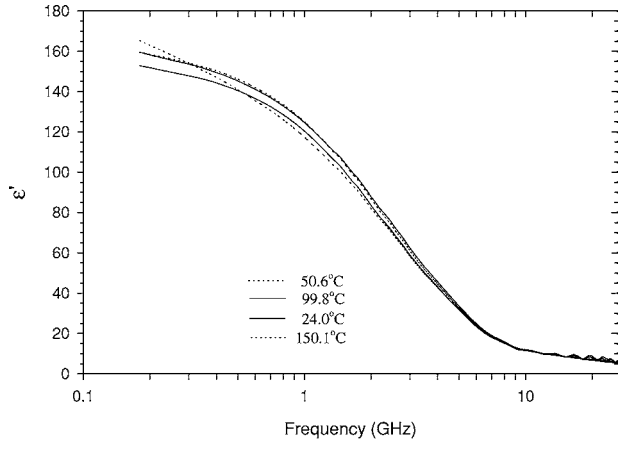

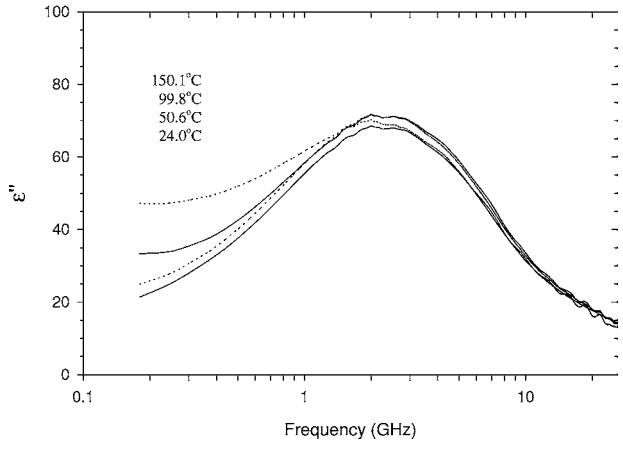

Figure 5 Carbopack Y: real (ε') and imaginary (ε'') components of complex permittivity.

space-charge polarizations [29–36]. Polarization-relaxation phenomena have been described by Debye as

$$\varepsilon^*(\omega) = \varepsilon_\infty + \frac{\varepsilon_s - \varepsilon_\infty}{1 + i\omega\tau} \tag{9}$$

where ε_s is the static (zero frequency) permittivity and τ represents the polarization relaxation time, which is the inverse of the frequency of maximum dielectric loss [29]. The real and imaginary components of the complex permittivity are then described as

$$\varepsilon'(\omega) = \varepsilon_\infty + \frac{\varepsilon_s - \varepsilon_\infty}{1 + (\omega\tau)^2} \tag{10}$$

$$\varepsilon''(\omega) = \frac{\varepsilon_s - \varepsilon_\infty}{1 + (\omega\tau)^2}\omega\tau \tag{11}$$

In the slightly more complex Cole-Cole model [30, 31] the $i\omega\tau$ term is raised to the power of β. Here, the individual permittivity terms [32] can be described as,

$$\varepsilon'(\omega) = \varepsilon_\infty + \frac{(\varepsilon_s - \varepsilon_\infty)}{2} \times \left[1 - \frac{\sinh(\beta \ln \omega\tau)}{\cosh(\beta \ln \omega\tau) + \cos\left(\frac{\beta\pi}{2}\right)}\right] \tag{12}$$

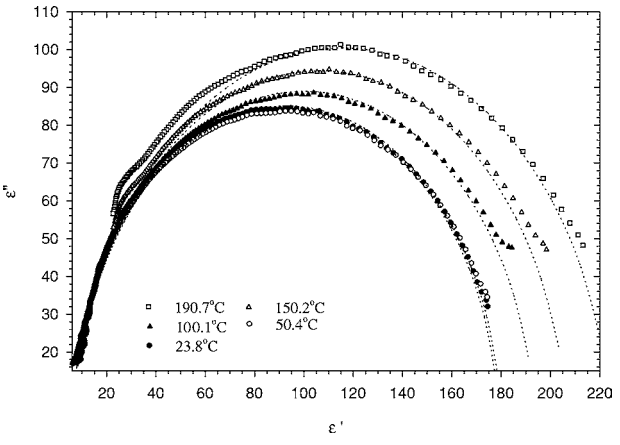

Figure 6 Cole-Cole plot for Carbopack B.

$$\varepsilon''(\omega) = \frac{(\varepsilon_s - \varepsilon_\infty)\sin\left(\frac{\beta\pi}{2}\right)}{2\left[\cosh(\beta \ln \omega\tau) + \cos\left(\frac{\beta\pi}{2}\right)\right]} \tag{13}$$

From these relations, it follows that a plot of ε'' versus ε' in the complex plane, termed a Cole-Cole plot, will form a semi-circle centered at,

$$\varepsilon'(\omega) = \frac{\varepsilon_s + \varepsilon_\infty}{2} \tag{14}$$

in which β is the central angle of circular arc for the dielectric loss.

Cole-Cole plots for the four graphitized carbon blacks are presented in Figs 6–9, respectively. In these representations, data are presented as symbols and the fit established using Equations 12 and 13 are shown as dashed lines. The derived polarization-relaxation parameters, including the relaxation time constants and values of β, are summarized in Table II. As shown in Fig. 6, the polarization-relaxation equation provides a reasonably good fit to the data acquired from the Carbopack B sample, using time constant (τ) values ranging between 6.86–7.96 $\times$ 10^{-11} s and values of β between 0.986–0.945. For Carbopack C (Fig. 7) the

TABLE II Summary of Cole-Cole polarization-relaxation parameters

Carbon black	T (°C)	τ (10^{-11} s)	β	ε_{rs}[a]	$\varepsilon_{r\infty}$[b]
Carbopack B	23.8	6.86	0.986	180	6
Carbopack B	50.4	6.86	0.986	179	6
Carbopack B	100.1	7.51	0.965	194	6
Carbopack B	150.2	7.96	0.960	206	6
Carbopack B	190.7	7.96	0.945	225	6
Carbopack C	23.6	2.59	1.00	155	2
Carbopack C	50.5	2.59	1.00	170	2.5
Carbopack X	23.8	5.13	0.82	102	2
Carbopack X	50.4	5.48	0.795	100	2
Carbopack X	99.3	5.48	0.772	99.8	2
Carbopack Y	24.0	7.73	0.93	155	2
Carbopack Y	50.6	7.96	0.93	162	2
Carbopack Y	99.8	7.96	0.93	164	2
Carbopack Y	150.1	7.96	0.93	160	2

[a] ε_{rs} is the relative static dielectric permittivity ($\varepsilon_s/\varepsilon_o$).
[b] $\varepsilon_{r\infty}$ is the relative dielectric permittivity at the high frequency limit ($\varepsilon_\infty/\varepsilon_o$).

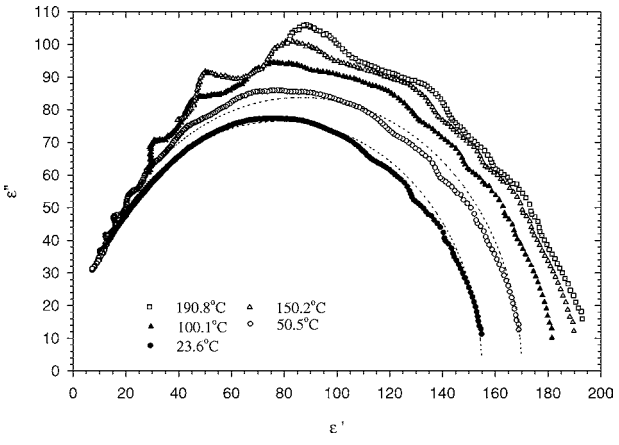

Figure 7 Cole-Cole plot for Carbopack C.

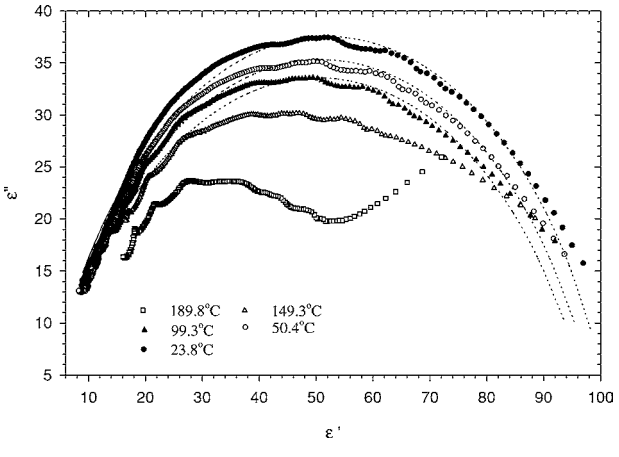

Figure 8 Cole-Cole plot for Carbopack X.

effects of the sinusoidal oscillations at high frequency are evident in the data taken at temperatures between 100.1–190.8°C. Here only the two lowest temperature curves are fitted to Equations 12 and 13. The relaxation time of 2.59×10^{-11} s corresponds to the significantly higher frequency of maximum dielectric loss for this material in comparison to the other three graphitized carbon blacks. Derived β values of 1.00 also indicate that these data fit the simpler Debye model given by Equations 10 and 11. In Fig. 8, the data for Carbopack X acquired at 23.8°C, 50.4°C, and 99.3°C are fitted to the polarization equations yielding relaxation times between 5.13–5.48 $\times$ 10^{-11} s and β values between 0.772–0.820. At higher temperatures the data indicate progressively increasing deviations at the low frequency end of the spectrum, resulting from electrical conductivity, which becomes significant at frequencies below 1.2 GHz at 189.8°C. In Fig. 9, fits of the Carbopack Y data for the three lowest temperatures are shown, yielding β values of 0.93 at all temperatures, and relaxation time constants between 7.73–7.96 $\times$ 10^{-11} s. Here too, significant deviation at the low frequency end of the spectrum is evident for the data acquired at 150.2°C. For all these materials, relaxation time constants either remain constant or increase with temperature, while β values either remain constant or decrease with temperature.

The deviation from semicircular symmetry, particularly at higher temperatures and lower frequencies, in these Cole-Cole plots is most likely due to the presence

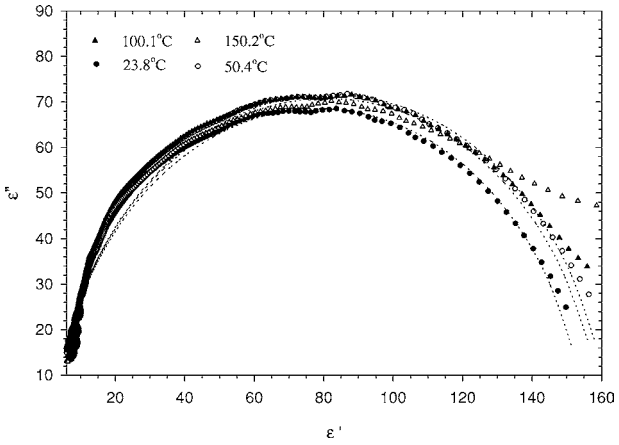

Figure 9 Cole-Cole plot for Carbopack Y.

of two or more independent dielectric relaxors. In the case of two relaxors

$$\varepsilon^*(\omega) = \varepsilon_\infty + \frac{A(\varepsilon_s - \varepsilon_\infty)}{1 + (i\omega\tau_1)^{\beta_1}} + \frac{(1-A)(\varepsilon_s - \varepsilon_\infty)}{1 + (i\omega\tau_2)^{\beta_2}} \tag{15}$$

where A is the fraction of polarizations corresponding to relaxor #1 and $1 - A$ is the fraction corresponding to relaxor #2. This situation can be generalized into systems of n independent relaxors, but analytically it becomes progressively more difficult to derive the corresponding relaxation times and β values.

4. Conclusions

Given the above, it is clear that all of the graphitized carbon blacks investigated exhibit strong microwave absorption characteristics across significant portions of the spectrum. It is also evident that substantial variability exists between materials, with frequencies of maximum dielectric loss ranging from 2.00–6.80 GHz. This can be attributed to the differences in source material and processing techniques. All of the Carbopacks are strongly susceptible to microwave heating at 0.915 and 2.45 GHz, the two most commonly used frequencies for industrial applications. For Carbopack C, the 2.45 GHz frequency can be used effectively, but for maximum efficiency frequencies between 4–10 GHz should be employed.

Acknowledgments

This work was funded by the Ames Research Center of the National Aeronautics and Space Administration under contract NAS2-97017. The authors are grateful to Dr. Bernadette K. Luna for her support of this project.

References

1. J. E. ATWATER and J. T. HOLTSNIDER, *SAE Trans.* **100** (1991) 1726.
2. R. L. PETTY, *Anal. Chem.* **53** (1981) 1548.
3. C. VIDAL-MADJAR, S. BERKASSY, M.F. GONNORD, P. ARPINO and G. GULOCHON, *ibid.* **49** (1977) 768.
4. A. DI CORCIA and M. GLABBAL, *ibid.* **50** (1978) 1000.

5. A. DI CORCIA and R. SAMPERI, *ibid.* **51** (1979) 776.
6. Z. KRAWLEC, M. F. GONNORD, G. GULOCHON and J. R. CHRETIEN, *ibid.* **51** (1979) 1655.
7. A. DI CORCIA, R. SAMPERI, E. SEBASTIANI and C. SEVERINI, *ibid.* **52** (1980) 1345.
8. A. BACALONI, G. GORETTI, B. M. PETRONIO and M. ROTATORI, *ibid.* **52** (1980) 2033.
9. J. NAMIESNIK, B. ZYGMUNT and A. JASTRZEBSKA, *J. Chromatogr.* A **885** (2000) 405.
10. C. BARONTI, R. CURINI, G. D'ASCENZO, A. DI CORCIA, A. GENTILI and R. SAMPERI, *Environ. Sci. Technol.* **34** (2000) 5059.
11. M. CONCEJERO, L. RAMOS, B. JIMENEZ, B. GOMARA, E. ABAD, J. RIVERA and M. J. GONZALEZ, *J. Chromatogr.* A **917** (2001) 227.
12. R. LOOS and D. BARCELO, *ibid.* **938** (2001) 45.
13. B. ZYGMUNT, A. JASTRZEBSKA and J. NAMIESNIK, *Crit. Rev. Anal. Chem.* **31** (2001) 1.
14. A. LAGANA, A. BACALONI, I. DE LEVA, A. FABERI, G. FAGO and A. MARINO, *Anal. Chim. Acta.* **462** (2002) 187.
15. F. PENA, S. CARDENAS, M. GALLEGO and M. VALCARCEL, *Talanta* **56** (2002) 727.
16. S. CUNNINGHAM and G. C. STEWART, *J. Amer. Soc. Brew. Chem.* **56** (1998) 12.
17. O. S. YOUNIS and G. C. STEWART, *ibid.* **57** (1999) 39.
18. J. E. ATWATER, J. T. HOLTSNIDER and R. R. WHEELER, JR., "Microwave Regenerable Air Purification Device" (National Technical Information Service, Springfield, Virginia, 1996).
19. A. VON HIPPEL, "Dielectrics and Waves" (Wiley, New York, 1954).
20. A. VON HIPPEL, "Dielectric Materials and Applications" (Technology Press of MIT, Cambridge, 1954).
21. A. K. JONSCHER, "Dielectric Relaxation in Solids" (Chelsea Dielectrics Press, London, 1983).
22. A. C. MATAXAS and R. J. MERIDITH, "Industrial Microwave Heating" (Peter Perigrinus, Ltd., London, 1983).
23. F. WANG, R. POTTEL and U. KAATZE, *J. Phys. Chem.* B **101** (1997) 922.
24. B. NOST, B. D. HANSEN and E. HASLUND, *Physica Scripta* **T44** (1992) 67.
25. D. POLDER and J. H. VAN SANTEN, *Physica* **12** (1946) 257.
26. A. STOGRYN, *IEEE Trans. Antennas Propagat.* **AP-32** (1984) 517.
27. L. S. TAYLOR, *ibid.* **AP-13** (1965) 943.
28. L. TSANG and J. A. KONG, *Radio Sci.* **16** (1981) 303.
29. P. DEBYE, "Polar Molecules" (Lancaster Press, Lancaster, Pennsylvania, 1929).
30. K. S. COLE and R. H. COLE, *J. Chem. Phys.* **9** (1941) 341.
31. D. W. DAVIDSON and R. H. COLE, *ibid.* **19** (1951) 1484.
32. T. OHGUSHI and K. ISIMARU, *Phys. Chem. Chem. Phys.* **3** (2001) 3229.
33. C. J. F. BOTTCHER, "Theory of Electric Polarization" (Elsevier, New York, 1952).
34. S. HAVRILIAK, JR. and S. J. HAVRILIAK, "Dielectric and Mechanical Relaxation in Materials" (Hanser, New York, 1997).
35. V. I. GAIDUK, "Dielectric Relaxation and Dynamics of Polar Molecules" (World Scientific, New Jersey, 1999).
36. A. K. JONSCHER, *J. Phys. D: Appl. Phys.* **32** (1999) R57.

Received 27 February
and accepted 12 August 2003